

Interplay between multiple charge-density waves and the relationship with superconductivity in Pd_xHoTe_3

Rui Lou,^{1,2} Yipeng Cai,^{1,2,*} Zhonghao Liu,^{3,†} Tian Qian,⁴ Lingxiao Zhao,⁴ Yu Li,⁵ Kai Liu,^{1,2} Zhiqing Han,^{1,2} Dandan Zhang,^{1,2} Junbao He,^{4,‡} Genfu Chen,^{4,6} Hong Ding,^{4,6} and Shancai Wang^{1,2,§}

¹*Department of Physics, Renmin University of China, Beijing 100872, China*

²*Beijing Key Laboratory of Opto-electronic Functional Materials & Micro-nano Devices, Renmin University of China, Beijing, China*

³*Institute for Solid State Research, IFW Dresden, Dresden 01171, Germany*

⁴*Beijing National Laboratory for Condensed Matter Physics, and Institute of Physics, Chinese Academy of Sciences, Beijing 100190, China*

⁵*Department of Physics and Astronomy, Rice University, Houston, Texas 77005, USA*

⁶*Collaborative Innovation Center of Quantum Matter, Beijing, China*

HoTe_3 , a member of the rare-earth tritelluride ($R\text{Te}_3$) family, and its Pd-intercalated compounds, Pd_xHoTe_3 , where superconductivity (SC) sets in as the charge-density wave (CDW) transition is suppressed by the intercalation of a small amount of Pd, are investigated using angle-resolved photoemission spectroscopy (ARPES) and electrical resistivity. Two incommensurate CDWs with perpendicular nesting vectors are observed in HoTe_3 at low temperatures. With a slight Pd intercalation ($x = 0.01$), the large CDW gap decreases and the small one increases. The momentum dependence of the gaps along the inner Fermi surface (FS) evolves from orthorhombicity to near tetragonality, manifesting the competition between two CDW orders. At $x = 0.02$, both CDW gaps decrease with the emergence of SC. Further increasing the content of Pd for $x = 0.04$ will completely suppress the CDW instabilities and give rise to the maximal SC order. The evolution of the electronic structures and electron-phonon couplings (EPCs) of the multiple CDWs upon Pd intercalation are carefully scrutinized. We discuss the interplay between multiple CDW orders, and the competition between CDW and SC in detail.

PACS numbers: 71.45.Lr, 71.18.+y, 79.60.-i

The recent observation of charge ordering in cuprate high-temperature superconductors^{1,2} has reignited interests in CDW and its interplay with SC. A new charge ordering is always introduced by different types of instabilities, such as lattice distortion or FS nesting. However, the driving force behind the CDW phase is still under debate.^{3–15} From a Peierls perspective, in an ideal one-dimensional (1D) system, the electronic susceptibility would develop a logarithmic divergence singularity at some sheets of the FSs spanning by nesting vectors via EPCs, and hence results in a phase transition to the CDW ground state accompanied by the commensurate/incommensurate periodic lattice distortions and the opening of energy gaps at E_F .^{3,4} Although, the quasi two-dimensional (2D) materials have a weaker tendency towards the nesting-driven CDWs owing to the imperfect nesting caused by the increased FS curvature, the electronic susceptibility could still be enhanced sufficiently for a CDW to develop under favorable nesting conditions and EPCs.^{16–19} Therefore, the CDW states in quasi 2D systems are particularly attractive due to the existence of possible multiple nesting properties and interacting collective orders added by the extra dimensionality.

The fairly simple electronic structure of $R\text{Te}_3$, where the CDW instabilities usually develop in the planar square nets of tellurium,¹⁴ provides an unprecedented opportunity to systematically investigate the CDW formation and its relationship with FS nesting under pretty accurate theoretical models. An incommensurate CDW

modulation characterized by a wave vector $\mathbf{q}_1 \approx 2/7\mathbf{c}^*$ was commonly observed.^{20–23} Recently, a second CDW transition occurs at lower temperatures with $\mathbf{q}_2 \approx 1/3\mathbf{a}^*$ perpendicular to the first was discovered in heavier members of $R\text{Te}_3$.^{19,23,24} Additionally, by the Pd intercalation, the suppression of CDWs and even the emergence of SC were observed.²⁵ Thus, this system offers the valuable possibility to explore the interplay between multiple CDW instabilities, and also between the CDW and SC orders. However, to date, little is known about the relationship of these orders belong to different collective phases. In order to obtain a much more comprehensive insight into the multiple CDWs formation and the interplay between various correlated electronic states, we performed high-resolution ARPES experiments on series of Pd_xHoTe_3 single crystals with the help of electrical transport measurements, focusing on the evolution of electronic structures and EPCs upon Pd intercalation. We provide the first systematic electronic structure study on the interplay between multiple CDWs, and their relationship with SC in $R\text{Te}_3$ family as a function of chemical intercalation.

Pd_xHoTe_3 single crystals with various nominal intercalated compositions ($x = 0, 0.01, 0.02$, and 0.04) are used in our study. In this paper, two incommensurate CDWs are identified. We observe the coexistence of two CDW gaps created by perpendicular nesting vectors in HoTe_3 at low temperature. The momentum dependence of the gaps along the inner FS reveals orthorhombicity. A slight

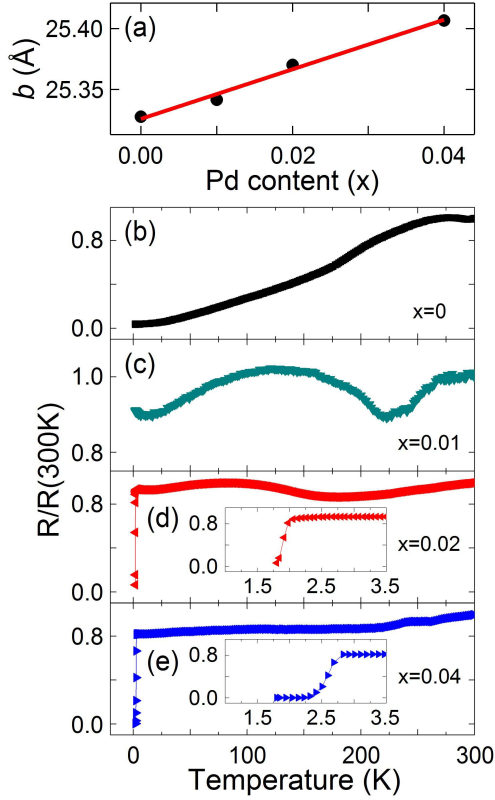


FIG. 1. (Color online) (a) Lattice parameter b as a function of x . The straight line is a guide to the eye. (b)-(e) Normalized temperature-dependent resistivity data measured on $x = 0$, 0.01, 0.02, and 0.04, respectively. Insets of (d),(e) are zoom in of $x = 0.02$ and 0.04 at low temperatures, respectively, showing the superconducting transitions.

Pd intercalation ($x = 0.01$) leads to remarkably different trends of these gaps, the gap symmetry turns out to be near tetragonality, proving the competition between the CDW orders. Both CDWs are further suppressed in $x = 0.02$, leading to the appearance of SC, and they vanish in $x = 0.04$, where the SC order reaches the maximum, showing the competition between CDW and SC. By quantitatively inspecting the evolution of electronic structures and EPCs, we demonstrate the nesting nature of multiple CDWs, suggest the significant increment of the second CDW gap from $x = 0$ to 0.01 determined by the EPC strength. The competition between these two CDWs, and their relationship with SC is very likely to be a FS competition scenario.

High-quality single crystals of Pd_xHoTe_3 were synthesized by the flux method.²⁶ ARPES measurements were performed at Renmin University of China and Institute of Physics, Chinese Academy of Sciences, with a He-discharge lamp, at the 1-cubed ARPES end station at BESSY and PGM beam line of the Synchrotron Radiation Center (Stoughton, WI). Spectra were recorded with 55 eV photons, taken at $T = 30$ K, with a pressure better than 4×10^{-11} Torr. Electrical transport measurements were performed in a PPMS-14 (Quantum Design).

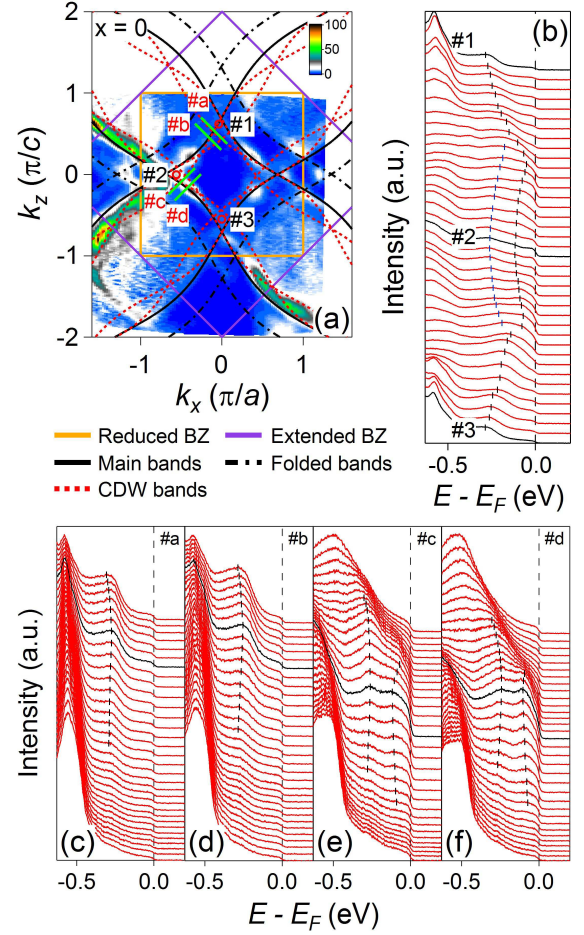


FIG. 2. (Color online) (a) ARPES intensity plot of HoTe_3 at E_F as a function of the 2D wave vector. The intensity is obtained by integrating the spectra within ± 15 meV with respect to E_F . The hopping parameters, t_{\parallel} and t_{\perp} , of the superimposed TB bands are ~ 1.85 and ~ 0.50 eV, respectively. (b) EDCs measured at various k_F points of the inner FS along #1–#2–#3, where #1, #2, and #3 are indicated by red circles in (a). The spectra at these three k_F points are highlighted by black curves. (c)-(f) EDC plots of cuts #a–#d indicated by green lines in (a), respectively. The CDW gap definitions and corresponding k_F positions are emphasized by black curves. Black and blue dashes in (b)-(f) are extracted peak positions, serving as guides to the eye.

As presented in Fig. 1(a), the monotonic increase of lattice constant b along with the increasing Pd content demonstrates the successful intercalation of Pd into the weakly bonded double Te layers. Figs. 1(b)-1(e) show the temperature dependence of electrical resistivity for Pd_xHoTe_3 . Consistent with previous work,²³ two bumps can be seen at ~ 290 and ~ 100 K in HoTe_3 , suggesting two well-separated CDW transitions. The second CDW transition at ~ 100 K is barely visible in the resistivity, this was interpreted as a renormalization of the electron dispersion in the ungapped FS parts, which may partially compensate the opening of the CDW gap on some FS sheets.²⁷ With the increasing amounts of Pd (x

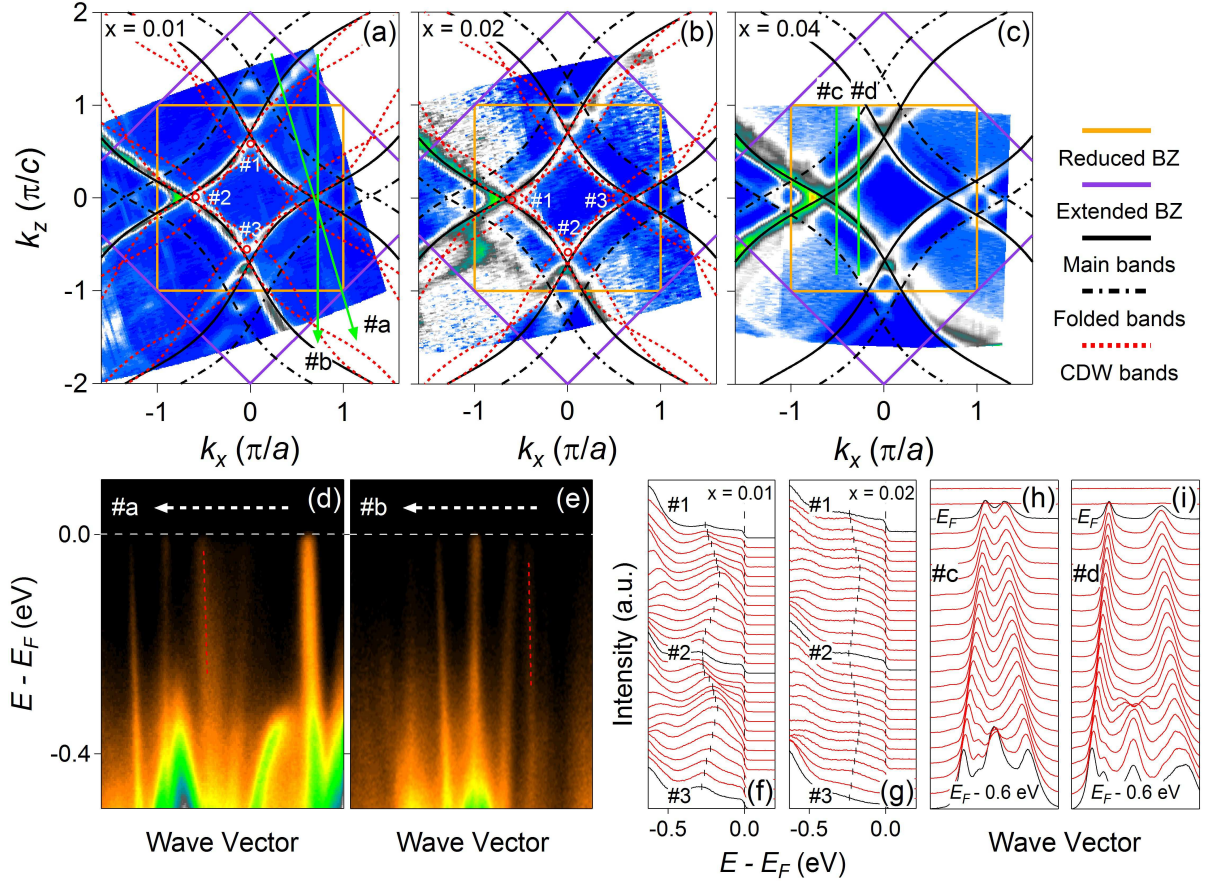


FIG. 3. (Color online) (a)-(c) FSs for $x = 0.01, 0.02$, and 0.04 , respectively, obtained by integrating the spectra within ± 15 meV with respect to E_F . The superimposed TB bands are calculated with the hopping parameters equally to that of HoTe_3 and fine adjustment of E_F values. (d),(e) ARPES intensity plots of $x = 0.01$ along cuts #a and #b, respectively, indicated by green arrows in (a). Red dashes are guides to the eye for the shadow bands. (f),(g) EDCs measured at various k_F points of the inner FS along #1–#2–#3, where #1, #2, and #3 are indicated by red circles in (a),(b), respectively. The spectra at these three k_F points are highlighted by black curves. Black dashes are extracted peak positions, serving as guides to the eye. (h),(i) Momentum distribution curve (MDC) plots of $x = 0.04$ along cuts #c and #d, respectively, indicated by green lines in (c).

$= 0.01$), these two CDWs exhibit opposite trends, two bumps merge at ~ 220 K. More clearly observed in the insets of Figs. 1(d) and 1(e), the SC emerges in $x = 0.02$ around 2.0 K with further suppressed CDW orders, and reaches the maximum (~ 2.8 K) in $x = 0.04$ accompanied by the vanished CDW instabilities, respectively.

We present in Fig. 2 the electronic structure of HoTe_3 . The FS in Fig. 2(a) is well described by a 2D tight-binding (TB) model including only the in-plane p_x and p_z orbitals of a Te plane, except at the crossings between them, owing to their interactions are neglected in our calculation. The dispersions for p_x and p_z can be readily derived as,

$$E_{p_x}(\mathbf{k}) = -2t_{\parallel} \cos[(k_x + k_z)\frac{a}{2}] + 2t_{\perp} \cos[(k_x - k_z)\frac{a}{2}] - E_F,$$

$$E_{p_z}(\mathbf{k}) = 2t_{\perp} \cos[(k_x + k_z)\frac{a}{2}] - 2t_{\parallel} \cos[(k_x - k_z)\frac{a}{2}] - E_F.$$

Details of the TB model are described elsewhere.⁸ The residual spectral distribution along the inner pocket,

which is similar to that in ErTe_3 ,¹⁹ indicates the existence of multiple CDWs characterized by different nesting vectors.

We choose two sets of cuts (#a,#b and #c,#d) to elucidate the different appearance of multiple CDW gaps, and present the corresponding energy distribution curves (EDCs) in Figs. 2(c)-2(f). Both cuts #a and #b show a back-bending band feature, this is reminiscent of the dispersion of Bogoliubov quasiparticles, suggesting the opening of a CDW gap. Instead, cuts #c and #d reveal both two quasiparticle branches, demonstrating the center of the CDW gap is pushed below E_F due to the longer than perfect nesting vector observed.^{4,19} As illustrated in Figs. 4(f) and 4(g) for Pd_xHoTe_3 , the definition of CDW gap is dependent on both the nesting conditions and EPC strength. For an ideal nesting, the CDW gap center locates at E_F , thus only the lower branches are visible; for an imperfect nesting with $q_n > q_{\text{CDW}}$, the gap center is pushed below E_F , moreover, if the coupling parameter (V) between these two nested states including EPCs is

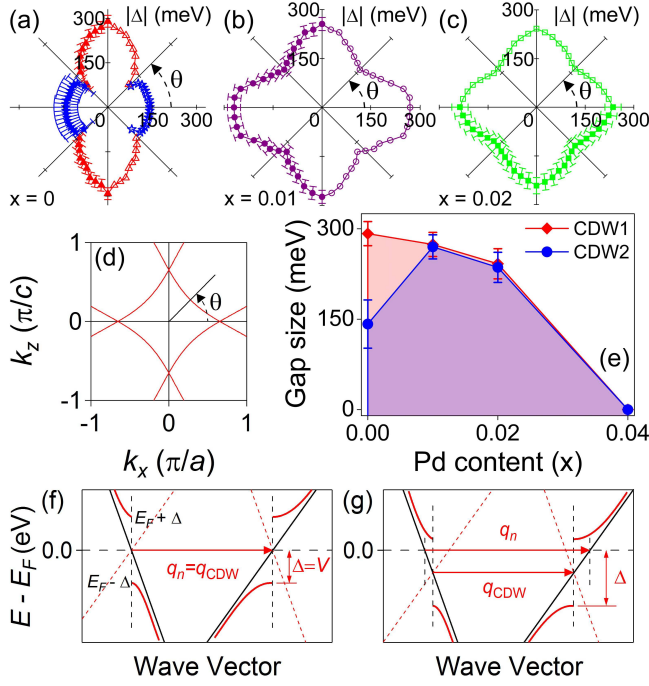


FIG. 4. (Color online) (a)-(c) Polar plots of the CDW gap size for the inner FS of $x = 0, 0.01$, and 0.02 , respectively, as a function of FS angle (θ) defined in (d). Filled symbols with error bars are the original data, consecutively extracted from the EDCs in Figs. 2(b), 3(f), and 3(g). Open symbols are the folded data which take into account the orthorhombic symmetry. (d) Schematic inner FS and definition of the FS angle (θ). (e) Summary of the two CDW gap magnitudes as a function of Pd intercalation, the values are extracted at the corners of the inner FSs. (f),(g) Schematic pictures illustrating two-band CDW intersection for Pd_xHoTe_3 when $q_n = q_{CDW}$ and $q_n > q_{CDW}$, respectively. Δ mixes two states in the unperturbed bands (thick black lines) connected by q_{CDW} , resulting in the gapped CDW bands indicated by thick red curves. The red dashed lines are translated bands by $\pm q_{CDW}$.

smaller than the binding energy of gap center, both two quasiparticle branches can be observed.^{3,6,8,18,28} Reasonably, the CDW gap definitions can be classified as, the gap between the lower branch and E_F is used for the situations with only lower branches visible, and the gap between these two branches is for the latter case, yielding $2V$. More details are discussed quantitatively below.

This apparent distinction indicates a second CDW gap different from that in cuts #a and #b. Detailed inspection on the binding energies of the branches at k_F reveals the decreasing trend from #a (~ 0.275 eV) to #b (~ 0.255 eV), and the same trend holds from #c (~ 0.121 eV) to #d (~ 0.103 eV), manifesting the shortened nesting vectors. To precisely determine the gap size and their momentum dependence, the EDCs at various k_F points of the inner FS along #1-#2-#3 are displayed in Fig. 2(b). Corresponding to the first gap definition, one can obtain a large CDW gap near the corners #1 and #3 with only lower branches observed, which gradually

decreases off the corners due to the imperfect nestings. And according to the second definition, a small CDW gap appears around #2 with its center below E_F , which approaches E_F when off the corner, and both two quasiparticle branches visible. These behaviors are consistent with the nesting-driven scenario.^{4,8,14,23}

To illustrate the characteristic of multiple CDWs and fully understand the interplay between them, we elaborate on the electronic structure evolution upon Pd intercalation. Figs. 3(a)-3(c) show the FS mapping data of $x = 0.01, 0.02$, and 0.04 , respectively. One can see the nearly fourfold symmetric intensity variation in the FSs of $x = 0.01$ and 0.02 rather than the apparent twofold symmetry in HoTe_3 , manifesting the symmetry of gap-opening connected to a CDW picture.^{17,29} The shadow bands sketched by red dashes in Figs. 3(d) and 3(e), indicated via cuts #a and #b in Fig. 3(a), respectively, also confirm the validity of FS nesting in determining the CDW instabilities in this system.

The detailed gap anisotropy study of $x = 0.01$ and 0.02 , like that of HoTe_3 in Fig. 2(b), are displayed in Figs. 3(f) and 3(g), respectively, revealing slightly orthorhombic, or nearly tetragonal symmetry, in stark contrast to the orthorhombicity in HoTe_3 . In the nesting-driven CDW picture, the origin of the intensity variation along the FS can be reasonably interpreted by the momentum dependence of these CDW gaps. We summarize the gap size along the inner FS of $x = 0, 0.01$, and 0.02 as a function of the FS angle (θ) in Figs. 4(a)-4(c), respectively, clearly confirming the anisotropy. It is noted that, as indicated by blue filled pentacles in Fig. 4(a), the definition of the second CDW gap in HoTe_3 is different from others' ascribed to the observation of both upper and lower quasiparticle branches. According to the different gap definitions discussed above, instead of the gap between the lower branch and E_F for others, we use the one between these two branches, characterized by $2V$.^{3,6,8,18,28}

We now discuss the nesting properties associated with the multiple gaps and spectral distribution along the FS. By comparing the nesting vectors determined by ARPES and TB model calculations with the x-ray diffraction results,²³ we can reasonably interpret the momentum dependence of the multiple CDW gaps and the gap center of the second CDW in HoTe_3 underlying E_F . For HoTe_3 , the two nesting vectors reveal $q_{n1} = c^* - q_{CDW1} \approx 0.71(3)c^*$ and $q_{n2} = a^* - q_{CDW2} \approx 0.69(5)a^*$, where the former is in complete agreement with the perfect nesting vector along c axis and the latter is longer than that along a axis, respectively. Thus, the center of the second CDW gap is pushed below E_F even at the corner (#2) of the inner FS, and gradually moves to lower binding energy with the shortened nesting vector.^{4,18,23} For $x = 0.01$ and 0.02 , the ones parallel to c axis are $0.68(8)$ and $0.67(1)c^*$, and to a axis are $0.68(4)$ and $0.67(3)a^*$, respectively, elucidating the FS topology becomes more isotropic upon Pd intercalation.

The evolution of the maximal gap size of the two CDW orders upon Pd intercalation are summarized in

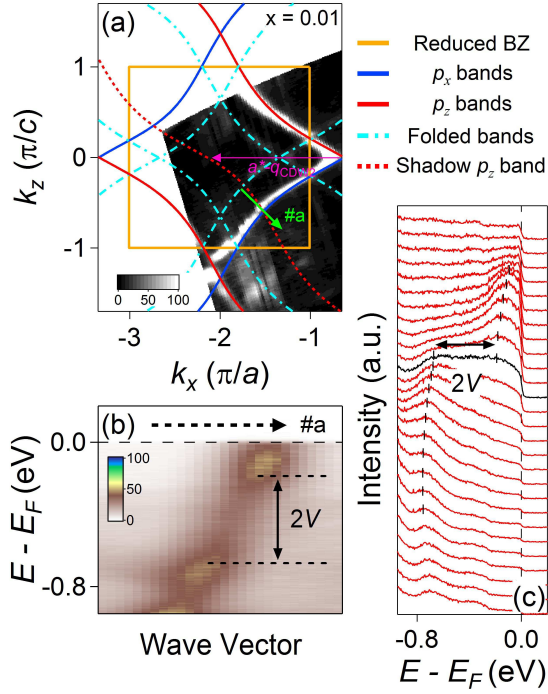


FIG. 5. (Color online) (a) FS for $x = 0.01$ around the second 3D (reduced) BZ center obtained by integrating the spectra within ± 15 meV with respect to E_F . The calculated TB bands with orbital projection and shadow p_z band are indicated to enable a study of the coupling strength between the states linked by a nesting vector, $\mathbf{a}^* - \mathbf{q}_{\text{CDW}2}$, shown as magenta arrow. (b) ARPES intensity plot measured at the crossing between p_x and shadow p_z bands along cut #a, indicated by green arrow in (a), and (c) corresponding EDC plot. The definition of $2V$ is emphasized by black curve. Black dashes are extracted peak positions, serving as guides to the eye.

Fig. 4(e). Combining the multiple nesting properties discussed above, it is conspicuous that upon Pd intercalation, the interplay between these two collective phases yields competition, similar to the optical spectroscopy results upon chemical pressure,³⁰ and to the transport measurements under pressure.^{31,32} These can to some extent be explicated by our multiple nesting properties, but not adequate yet. Along with the increasing Pd content, the first CDW gap gradually decreases ascribed to the shortened nesting vector. Simultaneously, the second CDW gap substantially increases for $x = 0.01$, and then decreases monotonically. The appreciable transform of the second CDW gap magnitude from $x = 0$ to 0.01 strongly suggests that, upon Pd intercalation, not only the FS evolution pointing to the nesting picture, but also the variation of EPC strength is needed to be fully included for investigating the interplay between multiple CDW orders quantitatively.

According to the above discussions, one can obtain the coupling strength (V) between the states linked by $\mathbf{a}^* - \mathbf{q}_{\text{CDW}2}$ in HoTe_3 from Fig. 2(b), where $2V = 0.142$ eV. However, as only the lower quasiparticle branch be-

ing observed in $x = 0.01$, one cannot determine the V unambiguously. Thus, we perform the measurements extended to the second three-dimensional (3D) BZ on $x = 0.01$, and illustrate the FS in Fig. 5(a). The dispersion presented in Fig. 5(b), indicated via cut #a in Fig. 5(a), is measured at the crossing between p_x and shadow p_z bands, of which the intensity is too weak to be clearly visible in the plot. It is distinct that a gap completely opens below E_F . Since these two states are coupled by a nesting vector, guided by magenta arrow in Fig. 5(a), the interaction between them would also yields the V .¹⁸ We now can precisely measure $2V$ using the corresponding EDC plot in Fig. 5(c), showing $2V = 0.484$ eV. Based on this, it is further confirmed that the EPC strength undergoes a significant variation from $x = 0$ to 0.01.

The detailed studies on the evolution of electronic structures and EPCs give us a high chance to extract the nature of the interplay between multiple CDWs, as well as their relationship with the SC in Pd_xHoTe_3 . According to the temperature versus pressure phase diagram proposed in Refs. 31 and 32, the role of Pd intercalation on the evolution of two CDWs and SC is similar to that of pressure performed on RTe_3 compounds. As already pointed out, the first CDW is suppressed monotonically because of the imperfect nesting. Simultaneously, the EPC strength of the second CDW has a remarkable transform from $x = 0$ to 0.01. This may be driven by the possible lattice distortion towards the tetragonal structure upon Pd intercalation, resulting from the competition between CDW orders for the low-energy spectral weight available for nesting.³⁰ Nevertheless, due to the longer than perfect nesting vector along a axis, the center of the second CDW gap still slightly locates below E_F in $x = 0.01$. Thus, the gap further decreases even with an ideal nesting vector in $x = 0.02$. The competition and suppression of these two CDW instabilities give rise to the emergence of SC in $x = 0.02$, then the SC order reaches the maximum with the vanished CDWs in $x = 0.04$. Extensive work has been carried on the interplay between CDW and SC, principally in cuprate high-temperature superconductors,^{1,2} yet the underlying mechanism for the competition is still controversial. Our ARPES results for the relationship between these collective states may shed light on it, even the high-temperature SC. As shown in the phase diagram of polycrystalline Pd_xHoTe_3 in Ref. 25, the weak Pd-intercalation dependence of T_c indicates the SC possibly not determined by quantum critical fluctuations, the competition for FS with CDWs based on the Bilbro-McMillan partial gapping scenario may be the dominant nature instead.^{31,33}

To conclude, we have performed ARPES and electrical transport experiments on Pd_xHoTe_3 single crystals to study the interplay between multiple CDWs and their relationship with SC. We report the systematic evolution of the electronic structures and EPCs upon Pd intercalation, determine the nesting-driven nature of the CDWs formation, and find the competition between these CDW

orders is for the low-energy spectral weight. The compelling evidences for the dramatic transform of EPC strength along a axis from $x = 0$ to 0.01 leave the effect of Pd intercalation further complicated, requiring future studies to clarify. The competition between SC and CDWs for the FS may provide insight into the microscopic origin of high-temperature SC, paving the way to identify more high-temperature superconductors.

We would like to thank Anmin Zhang, Yong Tian, and Qingming Zhang for helpful discussions, and Hechang Lei for the help in plotting figures. This work was funded by grants from the National Natural Science Foundation of China (Nos. 11274381 and 11404175), the National Basic Research Program of China (973 Program), the Ministry of Education of China, and the Chinese Academy of Sciences (No. XDB07000000).

-
- * Present address: Department of Physics, McMaster University, Hamilton, Ontario, L8S 4M1, Canada.
- † Present address: State Key Laboratory of Functional Materials for Informatic, SIMIT, Chinese Academy of Sciences, Shanghai 200050, China.
- ‡ Present address: Physics and Electronic Engineering College, Nanyang Normal University, Nanyang 473061, China. scw@ruc.edu.cn
- ¹ G. Ghiringhelli, M. Le Tacon, M. Minola, S. Blanco-Canales, C. Mazzoli, N. B. Brookes, G. M. De Luca, A. Frano, D. G. Hawthorn, F. He, T. Loew, M. M. Sala, D. C. Peets, M. Salluzzo, E. Schierle, R. Sutarto, G. A. Sawatzky, E. Weschke, B. Keimer, and L. Braicovich, *Science* **337**, 821 (2012).
 - ² E. H. da Silva Neto, P. Aynajian, A. Frano, R. Comin, E. Schierle, E. Weschke, A. Gyenis, J. Wen, J. Schneeloch, Z. Xu, S. Ono, G. Gu, M. Le Tacon, and A. Yazdani, *Science* **343**, 393 (2014).
 - ³ G. Grüner, *Rev. Mod. Phys.* **60**, 1129 (1988).
 - ⁴ G. Grüner, *Density Waves in Solids* (Addison-Wesley, Reading, MA, 1994).
 - ⁵ M. D. Johannes, I. I. Mazin, and C. A. Howells, *Phys. Rev. B* **73**, 205102 (2006).
 - ⁶ M. D. Johannes and I. I. Mazin, *Phys. Rev. B* **77**, 165135 (2008).
 - ⁷ F. Weber, S. Rosenkranz, J.-P. Castellan, R. Osborn, R. Hott, R. Heid, K.-P. Bohnen, T. Egami, A. H. Said, and D. Reznik, *Phys. Rev. Lett.* **107**, 107403 (2011).
 - ⁸ Hong Yao, John A. Robertson, Eun-Ah Kim, and Steven A. Kivelson, *Phys. Rev. B* **74**, 245126 (2006).
 - ⁹ B. Mansart, M. J. G. Cotter, T. Penfold, S. Dugdale, R. Tediosi, M. Chergui, and F. Carbone, *Proc. Natl. Acad. Sci. USA* **109**, 5603 (2012).
 - ¹⁰ D. S. Inosov, V. B. Zabolotnyy, D. V. Evtushinsky, A. A. Kordyuk, B. Büchner, R. Follath, H. Berger, and S. V. Borisenko, *New J. Phys.* **10**, 125027 (2008).
 - ¹¹ K. Rossnagel, *J. Phys.: Condens. Matter* **23**, 213001 (2011).
 - ¹² J. Dai, E. Calleja, J. Alldredge, X. Zhu, L. Li, W. Lu, Y. Sun, T. Wolf, H. Berger, and K. McElroy, *Phys. Rev. B* **89**, 165140 (2014).
 - ¹³ C. J. Arguello, E. P. Rosenthal, E. F. Andrade, W. Jin, P. C. Yeh, N. Zaki, S. Jia, R. J. Cava, R. M. Fernandes, A. J. Millis, T. Valla, R. M. Osgood, Jr., and A. N. Pasupathy, *Phys. Rev. Lett.* **114**, 037001 (2015).
 - ¹⁴ J. Laverock, S. B. Dugdale, Zs. Major, M. A. Alam, N. Ru, I. R. Fisher, G. Santi, and E. Bruno, *Phys. Rev. B* **71**, 085114 (2005).
 - ¹⁵ S. Kawasaki, Y. Tani, T. Mabuchi, K. Kudo, Y. Nishikubo, D. Mitsuoka, M. Nohara, and G.-Q. Zheng, *Phys. Rev. B* **91**, 060510(R) (2015).
 - ¹⁶ G.-H. Gweon, J. D. Denlinger, J. A. Clack, J. W. Allen, C. G. Olson, E. D. DiMasi, M. C. Aronson, B. Foran, and S. Lee, *Phys. Rev. Lett.* **81**, 886 (1998).
 - ¹⁷ V. Brouet, W. L. Yang, X. J. Zhou, Z. Hussain, N. Ru, K. Y. Shin, I. R. Fisher, and Z. X. Shen, *Phys. Rev. Lett.* **93**, 126405 (2004).
 - ¹⁸ V. Brouet, W. L. Yang, X. J. Zhou, Z. Hussain, R. G. Moore, R. He, D. H. Lu, Z. X. Shen, J. Laverock, S. B. Dugdale, N. Ru, and I. R. Fisher, *Phys. Rev. B* **77**, 235104 (2008).
 - ¹⁹ R. G. Moore, V. Brouet, R. He, D. H. Lu, N. Ru, J.-H. Chu, I. R. Fisher, and Z. X. Shen, *Phys. Rev. B* **81**, 073102 (2010).
 - ²⁰ E. DiMasi, M. C. Aronson, J. F. Mansfield, B. Foran, and S. Lee, *Phys. Rev. B* **52**, 14516 (1995).
 - ²¹ C. D. Malliakas and M. G. Kanatzidis, *J. Am. Chem. Soc.* **128**, 12612 (2006).
 - ²² N. Ru and I. R. Fisher, *Phys. Rev. B* **73**, 033101 (2006).
 - ²³ N. Ru, C. L. Condon, G. Y. Margulis, K. Y. Shin, J. Laverock, S. B. Dugdale, M. F. Toney, and I. R. Fisher, *Phys. Rev. B* **77**, 035114 (2008).
 - ²⁴ B. F. Hu, B. Cheng, R. H. Yuan, T. Dong, A. F. Fang, W. T. Guo, Z. G. Chen, P. Zheng, Y. G. Shi, and N. L. Wang, *Phys. Rev. B* **84**, 155132 (2011).
 - ²⁵ J. B. He, P. P. Wang, H. X. Yang, Y. J. Long, L. X. Zhao, C. Ma, D. M. Wang, X. C. Shangguan, Z. A. Ren, J. Q. Li, and G. F. Chen, *arXiv:1301.3032*.
 - ²⁶ F. Pfanner, P. Lerch, J.-H. Chu, H.-H. Kuo, I. R. Fisher, and L. Degiorgi, *Phys. Rev. B* **81**, 195110 (2010).
 - ²⁷ A. A. Sinchenko, P. D. Grigoriev, P. Lejay, and P. Monceau, *Phys. Rev. Lett.* **112**, 036601 (2014).
 - ²⁸ J. Voit, L. Perfetti, F. Zwick, H. Berger, G. Margaritondo, G. Grüner, H. Höchst, and M. Grioni, *Science* **290**, 501 (2000).
 - ²⁹ As proposed in Ref. 16, the residual spectral weight near E_F in the gapped FS sheets is caused by the photoelectron spectroscopy peak's linewidth tail, which arises from the thermal CDW fluctuations, phonon broadening or photoelectron lifetime, and some non- \mathbf{k} -conserving scattering possibly.
 - ³⁰ B. F. Hu, B. Cheng, R. H. Yuan, T. Dong, and N. L. Wang, *Phys. Rev. B* **90**, 085105 (2014).
 - ³¹ J. J. Hamlin, D. A. Zocco, T. A. Sayles, M. B. Maple, J.-H. Chu, and I. R. Fisher, *Phys. Rev. Lett.* **102**, 177002 (2009).
 - ³² D. A. Zocco, J. J. Hamlin, K. Grube, J.-H. Chu, H.-H. Kuo, I. R. Fisher, and M. B. Maple, *Phys. Rev. B* **91**, 205114 (2015).
 - ³³ G. Bilbro and W. L. McMillan, *Phys. Rev. B* **14**, 1887 (1976).